Title
Bioinspired Di-Fe Complexes: Correlating Structure and Proton Transfer over Four Oxidation States

Journal
Journal of the American Chemical Society, 144(10)

ISSN
0002-7863

Authors
Lee, Justin L
Biswas, Saborni
Sun, Chen
et al.

Publication Date
2022-03-16

DOI
10.1021/jacs.1c12888

Peer reviewed

HHS Public Access

Author manuscript

J Am Chem Soc. Author manuscript; available in PMC 2022 July 05.

Published in final edited form as:

J Am Chem Soc. 2022 March 16; 144(10): 4559–4571. doi:10.1021/jacs.1c12888.

Bioinspired Di-Fe Complexes: Correlating Structure and Proton Transfer over Four Oxidation States

Justin L. Lee[†], **Saborni Biswas**[⊥], **Chen Sun**[†], **Joseph W. Ziller**[†], **Michael P. Hendrich**[⊥], **A.S. Borovik**[†]

[†] Department of Chemistry, 1102 Natural Sciences II, University of California, Irvine, CA 92697

[⊥] Department of Chemistry, Carnegie Mellon University, 4400 Fifth Avenue, Pittsburgh, PA 15213

Abstract

Metalloproteins with active sites containing di-Fe cores exhibit diverse chemical reactivity that are linked to the precise transfer of protons and electrons which directly involve the di-Fe units. The redox conversions are commonly corroborated by spectroscopic methods, but the associated structural changes are often difficult to assess, particularly those related to proton movements. This report describes the development of di-Fe complexes in which the movements of protons and electrons are pinpointed during the stepwise oxidation of a di-Fe^{II} species to one with an $Fe^{III}Fe^{IV}$ core. Complex formation was promoted using the phosphinic amido tripodal ligand $[poat]^{3-}$ (*N,N′,N″*-[nitrilotris(ethane-2,1-diyl)]tris(*P,P*-diphenylphosphinic amido)) that provided dynamic coordination spheres that assisted in regulating both electron and proton transfer processes. Oxidation of an $[Fe^{II}$-(μ-OH)-$Fe^{III}]$ complex led to the corresponding di-Fe^{III} species containing an hydroxido bridge that was not stable at room temperature and converted to a species containing an oxido bridging ligand and protonation of one phosphinic amido group to form $[Hpoat]^{2-}$. Deprotonation led to a new species with an $[Fe^{III}$-(μ-O)-$Fe^{III}]$ core that could be further oxidized to its $Fe^{III}Fe^{IV}$ analog. Reactions with phenols suggest homolytic cleavage of the O–H bond to give products that are consistent with the initial formation of a phenoxyl radical —spectroscopic studies indicated that the electron is transferred to the Fe^{IV} center and the proton is initially transferred to the more sterically hindered oxido ligand but then relocates to $[poat]^{3-}$. These findings offer new mechanistic insights related to the stability of and the reactions performed by di-Fe enzymes.

Graphical Abstract

Corresponding Authors aborovik@uci.edu, hendrich@andrew.cmu.edu.

The authors declare no competing financial interests.

ASSOCIATED CONTENT

Supporting Information

The Supporting Information is available free of charge on the ACS Publication website at DOI:

The following file is available free of charge.

Experimental descriptions and characterization data for all new compounds, Figures S1–S17, and details of the crystallographic data in Table S1 (PDF).

Accession Codes

CCDC 2121051-2121053 contain the supplementary crystallographic data for this paper. These data can be obtained free of charge via www.ccdc.cam.ac.uk/data_request/cif, or by emailing data_request@ccdc.cam.ac.uk, or by contacting The Cambridge Crystallographic Data Centre, 12 Union Road, Cambridge CB2 1EZ, UK; fax: +44 1223 336033.

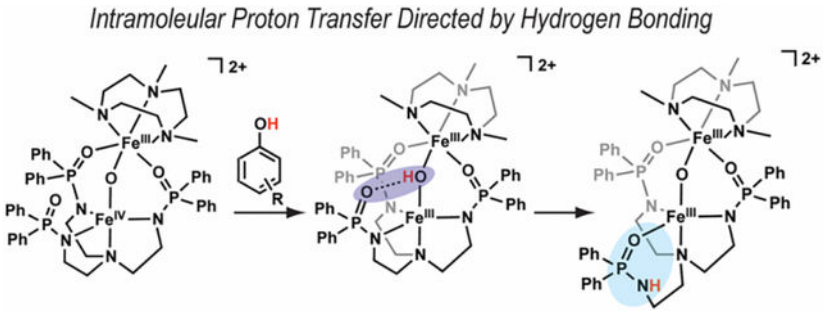

Introduction

Controlled proton and electron transfer processes within the active sites of metalloproteins are often necessary for function and to thwart undesirable reactivity.[1–4] The productive balance of these transfer processes is often managed by metallocofactors whose properties are regulated through a combination of effects at their primary and secondary coordination spheres.[5–7] Determining the interplay between these two coordination spheres is a necessary prerequisite before a complete mechanistic understanding of function can be achieved. To investigate these questions within systems containing di-Fe centers, we have developed a synthetic di-Fe^{II} species that can be oxidized in discrete one-electron steps to an $Fe^{IV}Fe^{III}$ species. This system is also able to control proton transfer via intramolecular processes, which increases the stability of the higher valent species and provides probes for studying biological oxidative chemistry.

Metalloproteins with di-Fe centers have a range of functions that include hemerythrin for O_2 binding,[8] soluble methane monooxygenase hydroxylase (MMOH)[9] and the R2 subunit of class Ia ribonucleotide reductases (RNR R2)[10–13] for O_2 activation, flavin diiron proteins (FDP) for NO and O_2 reduction,[14,15] and Δ^9-desaturatase for oxidation of fatty acid chains.[16,17] Oxidation of the di-Fe centers are often accompanied by structural changes that include the transfer of protons from coordinated ligands (e.g., OH^- and H_2O).[18,19] These proton/electron transfer steps, and how they are linked, are often proposed in mechanisms but rarely supported by experimental evidence. For instance, the mechanism for RNR R2 includes the conversion of the resting di-Fe^{II} state to an $Fe^{IV}Fe^{III}$ intermediate (X) that is able to homolytically cleave the O–H bond at nearby tyrosine residue to form a tyrosine radical, triggers a long-range electron transfer process (> 35 Å) that extends to the R1 subunit, where ribonucleotides are reduced to deoxyribonucleotides (Figure 1A).[11,20,21] Synthetic complexes have been developed to probe the properties of these intermediates. In particular, di-Fe^{IV} and $Fe^{IV}Fe^{III}$ complexes have been prepared and studied.[22–31] However, thermodynamic parameters that govern the formation of these complexes from their lower valent precursors are lacking. In addition, the associated structural changes that occur upon oxidation are also rarely known.

We have approached this problem by developing an assembly process to preparing complexes with discrete di-Fe cores. One advantage of our approach is that we can use well-defined monomeric complexes which allow us to prepare di-Fe cores with different primary coordination sphere around each Fe center. This approach is made possible by

the use of the multi-functional tripodal ligand $[poat]^{3-}$ (*N,N′,N″*-[nitrilotris(ethane-2,1-diyl)]tris(*P,P*-diphenylphosphinic amido)) that we initially designed to stabilize high valent Fe^{IV}=O complexes (Figure 1B).[32] We discovered that $[Fe^{III}poat(OH)]^-$ and $[Fe^{IV}poat(O)]^-$ complexes are able to bind a second Fe complex via coordination to the O/OH ligand and two P=O units, producing triply bridge species that resemble di-Fe core found in biology (Figure 1A). In this report we describe the preparation and properties of a series of complexes with either [Fe–(μ-OH)–Fe] or [Fe–(μ-O)–Fe] cores that traverse four different oxidation levels (Figure 1C). Our work demonstrates that $[poat]^{3-}$ can be used to control PT processes that occur during oxidation and provides access to a high valent [Fe^{IV}–(μ-O)–Fe^{III}] complex, which we used to examine the cleavage of X–H bonds, including reactions that are similar to those found within the active site of RNR R2. Our findings suggest an alternate mechanism for reactivity of X towards tyrosine, in which initial proton transfer first occurs at the oxido ligand that bridges between the two Fe centers, then proceeds to the terminal OH ligand on the Fe^{III} center.

Results

[(TMTACN)Fe^{II}–(μ-OH)–Fe^{III}poat]OTf and [(TMTACN)Fe^{II}–(μ-OH)–Fe^{II}poat].

We have previously prepared a mixed-valent $Fe^{II}Fe^{III}$ complex, [(TMTACN)Fe^{II}–(μ-O)–Fe^{III}MST]$^+$ ([Fe^{II}(OH)Fe^{III}MST]$^+$), in which an Fe^{III} center is bound to the sulfonamido-based tripodal ligand $[MST]^{3-}$ (*N,N',N"*-[2,2',2"-nitrilotris(ethane-2,1-diyl)]tris(2,4,6-trimethylbenzenesulfonamido)), and the Fe^{II} site is capped by an N-based macrocycle [TMTACN] (1,4,7-trimethyl-1,4,7-triazacyclononane).[33,34] However, we were not able to explore further oxidation of this complex, and our studies suggested that the sulfonamido groups were not suitable for stabilizing higher oxidation states. To circumvent this problem, we redesigned the ligand framework to include phosphinic amido group and recently reported that $[poat]^{3-}$ can facilitate the formation of the high valent species $[Fe^{IV}poat(O)]^-$ complex which can further bind group 2 metal ions.[32] In addition, we discovered that heterobimetallic complexes with the general formula of [(TMTACN)M^{II}–(μ-OH)–Fe^{III}poat]$^+$ (M^{II} = Ni, Cu, Zn, Mg) can be prepared.[35,36] We found that the same synthetic route provided access to di-Fe complexes and we initially synthesized [(TMTACN)Fe^{II}–(μ-OH)–Fe^{III}poat]OTf ([Fe^{II}(OH)Fe^{III}poat]OTf) (Scheme 1). In a typical reaction, NMe_4OAc was added to a CH_2Cl_2 solution of K[Fe^{III}poat(OH)] in a salt metathesis reaction. Upon removal of the insoluble KOAc, [Fe^{II}(TMTACN)$(OTf)_2$] was added to the mixture to produce the bimetallic compound. The [Fe^{II}(OH)Fe^{III}poat]OTf salt was initially purified as a powder from a diethyl ether-CH_2Cl_2 mixture, and then further purified as yellow sheet-like crystals from a hexane-CH_2Cl_2 mixture. The complex exhibits absorbance features at λ_{max} (ε, M^{-1} cm^{-1}) = 315 (sh), 372 (6400), 460 (sh), and 520 nm (sh) (Figure S1). The LMCT absorbance feature at λ_{max} = 372 nm is similar to those previously reported in our related bimetallic complexes with $[MST]^{3-}$ and $[poat]^{3-}$ ligands.[34,35] The FTIR spectrum of the [Fe^{II}(OH)Fe^{III}poat]OTf salt revealed a weak vibrational feature at 3141 cm^{-1}, which we assigned to the ν(O–H) band that forms a strong intramolecular H-bond to the P=O group in $[poat]^{3-}$ (Figure S2A).

Electron paramagnetic resonance (EPR) spectroscopy reveals a rhombic $S = 1/2$ signal with features at $g = 1.95$, 1.49, and 1.20 (Figure S3). These parameters agree with the assignment of an $S = 5/2$ Fe^{III} center antiferromagnetically coupled to an $S = 2$ Fe^{II} center. Throughout this work, the di-Fe complexes have been analyzed with ^{57}Fe Mössbauer spectroscopy in variable magnetic fields and temperatures. The details of these investigations will be described in a separate report – presented here are the values of the isomer shifts (δ), quadrupole splittings (ΔE_Q) and exchange coupling constants ($+J(S_1 \cdot S_2)$) that determined oxidation states of the specific Fe centers and protonation state of the single-atom bridge. The Mössbauer spectrum of $[^{57}Fe^{II}(OH)^{57}Fe^{III}poat]^+$ gave two distinct doublets with $\delta =$ 0.34 mm/s, $\Delta E_Q = -0.72$ mm/s and $\delta = 1.20$, $\Delta E_Q = -2.84$ mm/s for the two Fe sites (Figure S4A). These parameters are consistent with high spin $[Fe^{III}poat]$ and high spin $[Fe^{II}(TMTACN)]$, respectively.[37] Temperature and field-dependent measurements of this species revealed an exchanged-coupled $S = 1/2$ system with $J = 30$ cm^{-1}; the magnitude of J is consistent with a hydroxido bridging ligand.[38]

The molecular structure of $[Fe^{II}(OH)Fe^{III}poat]^+$ was determined by X-ray diffraction methods and revealed a discrete bimetallic structure (Figure 2A,S5A). There are two crystallographically different, but chemically equivalent, molecules in the asymmetric unit and we will discuss the averages of the metrical parameters and calculated values, which are shown in Table 1. The Fe^{III} site in the $[poat]^{3-}$ framework adopts a trigonal bipyramidal geometry with an N_4O primary coordination sphere, comprising of the $[poat]^{3-}$ ligand and a bridging hydroxido ligand ($\tau_5 = 0.884$, where the ideal trigonal bipyramidal geometry has a $\tau_5 = 1$, and the ideal square pyramidal geometry has a $\tau_5 = 0$). The Fe^{II} site in the Fe-TMTACN adduct is 6-coordinated with an N_3O_3 primary coordination sphere, comprising of the TMTACN ligand, two phosphinic amido groups from the $[poat]^{3-}$ ligand, and a bridging hydroxido ligand. The significantly different Fe1–O1 and Fe2–O1 bond lengths of 1.894(1) and 2.015(2) Å agree with the results from our spectroscopic studies and reflects the distinct oxidation states of the two Fe centers. The di-Fe center in $[Fe^{II}(OH)Fe^{III}poat]^+$ is best described as a triply bridge core with an Fe^{II}–(μ-OH)–Fe^{III} unit and two phosphinic amido bridges between the two Fe centers. The remaining phosphinic amido tripodal arm that does not bind to the Fe^{II} site forms an intramolecular H-bond with the hydroxido ligand with an O1···O2 distance of 2.649(2) Å. The metrical parameters around the Fe centers are comparable with those previously reported for the Zn/Cu/Ni/Mg analogs.[35,36] In addition, the Fe^{II}–O=P bond lengths (Fe2–O3, 2.094(1) and Fe2–O4, 2.124(1) Å) are significantly shorter than those for Fe^{II}–O=S in $[Fe^{II}(OH)Fe^{III}MST]^+$ (2.201(2) and 2.202(2) Å),[34] which supports the premise that phosphinic amido P=O groups serve as stronger donors and may support the Fe center at a higher oxidation state.

The electrochemical properties of $[Fe^{II}(OH)Fe^{III}poat]^+$ were investigated using cyclic voltammetry. The $[Fe^{II}(OH)Fe^{III}poat]^+$ complex exhibited two reversible one-electron redox events at −1.62 V and −0.42 V vs. $[Fe^{III/II}Cp_2]^{+/0}$, which are assigned to the $Fe^{II}Fe^{III}$/$Fe^{II}Fe^{II}$ and $Fe^{III}Fe^{III}$/$Fe^{II}Fe^{III}$ couples, respectively (Figure 3). These potentials are −0.7 V more negative than the same processes in the MST analog (−0.86 and +0.35 V).[33] While it has been previously shown that the trianionic equatorial N-plane can support a higher-valent metal center (e.g., Fe^{IV}),[32] these electrochemical results suggest experimentally that the

P=O moieties can also readily support a metal ion beyond the +2 state in the auxiliary binding site.

We explored the chemical reduction of $[Fe^{II}(OH)Fe^{III}poat]^{+}$ using $CoCp^*_2$ ($E_{1/2}$ = −1.94 V vs. $[FeCp_2]^{+/0}$)[39] as the reductant (Scheme 2) and found a nearly featureless electronic absorption spectrum in the visible region (Figure S6). The ^{57}Fe Mossbauer spectrum displayed two distinct quadrupole doublets with δ = 1.03 mm/s, $|\Delta E_Q|$ = 3.38 mm/s and δ = 1.22 mm/s, $|\Delta E_Q|$ = 2.37 mm/s which are typical of high spin Fe^{II} centers (Figure S4B). Variable-temperature Mössbauer studies in high magnetic field determined an antiferromagnetic exchange coupling of J = 20 cm^{-1} between the Fe^{II} sites which indicates the presence of a bridging hydroxido ligand.[38] The complex was EPR-silent consistent with an S = 0 ground state caused by the antiferromagnetic interaction. The nearly insignificant change of 0.02 mm/s in the value of δ for the Fe^{II}(TMTACM) site indicates that the Fe coordinated to the poat ligand is being reduced. These values are consistent with the formulation [(TMTACN)Fe^{II}–(μ-OH)–Fe^{II}poat]; however, several attempts to isolate a pure solid of this complex were unsuccessful with only $[Fe^{II}(OH)Fe^{III}poat]^{+}$ being obtained. We therefore focused our investigations on the oxidative chemistry associated with $[Fe^{II}(OH)Fe^{III}poat]^{+}$.

[(TMTACN)Fe^{III}–(μ-O)–Fe^{III}Hpoat](OTf)$_2$. Synthesis and Structure.

The chemical oxidation of $[Fe^{II}(OH)Fe^{III}poat]$OTf was achieved using $[FeCp_2]$OTf (Scheme 3) to afford orange crystals after purification. The electron spray ionization mass spectrum of these crystals dissolved in CH_3CN contains the molecular weight and experimental isotope pattern that matched those calculated for $\{[Fe^{III}(OH)Fe^{III}poat](OTf)\}^{+}$ (Figure S7A,C). However, ESI-MS data alone cannot determine the molecular structure of di-Fe^{III} complex, particularly whether the proton is still on the bridging ligand. To address this question, we determined its molecular structure via XRD methods to again find a triply bridged di-Fe complex but one with an Fe^{III}–(μ-O)–Fe^{III} core, [(TMTACN)Fe^{III}–(μ-O)–Fe^{III}Hpoat](OTf)$_2$ ($[Fe^{III}(O)Fe^{III}Hpoat](OTf)_2$); Figure 2B,S5B; Table 1). Unlike in $[Fe^{II}(OH)Fe^{III}poat]^{+}$, the Fe1–O1 and Fe2–O1 bond distances of 1.800(1) and 1.792(1) Å in $[Fe^{III}(O)Fe^{III}Hpoat]^{2+}$ are within statistical error, which is often observed in μ-oxido diiron(III) systems.[18,37,38] Two phosphinic amido groups of $[Hpoat]^{2-}$ serving as 3-atom bridging ligands and the Fe–O–Fe unit is bent at an angle of 124.73(8)°, which is similar to that observed in $[Fe^{II}(OH)Fe^{III}poat]^{-}$; however, contraction of the Fe–O bonds led to a decrease in the Fe···Fe distance from 3.436(1) to 3.182(1) Å. These metrical parameters are consistent with other triply-bridged μ-oxido diiron(III) complexes that have been reported in the literature.[38,40–43]

The conversion of species with Fe^{II}–(μ-OH)–Fe^{n} cores (n = II, III) to those with Fe^{III}–(μ-O)–Fe^{III} cores is known, presumably because the increased acidity of hydroxido proton unit upon oxidation results in the deprotonation. However, either an external base is needed to scavenge the proton or its whereabouts are unknown.[8,44–49] Within this context, the structure of $[Fe^{III}(O)Fe^{III}Hpoat]^{2+}$ is distinct in that one of phosphinic amido tripodal arms is protonated at its N-atom to form $[Hpoat]^{2-}$, causing a change to an N_3O_2 primary coordination sphere in which the P=O moiety is now bounded to the Fe^{III} center with an

Fe1–O2 bond length of 2.016(1) Å. This binding mode results in a strained 7-member chelate ring, and a large distortion in the trigonal plane, as evidenced by a τ_5 value of 0.734. The Fe^{III} site in Fe-TMTACN maintains the same N_3O_3 primary coordination sphere, comprising of the TMTACN ligand, two phosphinic amido groups from the $[Hpoat]^{2-}$ ligand, and a bridging oxido ligand.

Spectroscopic Studies on $[Fe^{III}(O)Fe^{III}Hpoat]^{2+}$.

$[Fe^{III}(O)Fe^{III}Hpoat]^{2+}$ was EPR-silent which indicated a magnetically coupled di-Fe^{III} core. Mössbauer spectroscopy on ^{57}Fe-enriched samples were analyzed in both solution and solid-state. The solution sample displayed an identical spectrum as the solid-state sample, indicating that the $[Fe^{III}(O)Fe^{III}Hpoat]^{2+}$ complex retains its molecular structure in solution. Two distinct doublets were observed in the Mössbauer spectra from $S = 5/2$ Fe^{III} centers (Figure S4C). One doublet site with $\delta = 0.49$ mm/s and $|\Delta E_Q| = 1.83$ mm/s corresponds to a six-coordinate Fe^{III} center and was therefore assigned to the iron in the auxiliary binding site. The other doublet with $\delta = 0.44$ mm/s and $|\Delta E_Q| = 1.26$ mm/s is from the 5-coordinate Fe^{III} center which is coordinated to the $[Hpoat]^{2-}$ ligand. Variable-temperature Mössbauer studies in high magnetic field gave an antiferromagnetic exchange coupling of $J > 100$ cm^{-1} which is expected for complexes with antiferromagnetically coupled Fe–(μ-O)–Fe cores.[38] $[Fe^{III}(O)Fe^{III}Hpoat]^{2+}$ has electronic absorption features at λ_{max} (ε, M^{-1} cm^{-1}) = 380 (7000), 517 (970), and 705 nm (130) that are comparable with previously reported tri-bridged μ-oxido di-Fe^{III} species with Fe–O–Fe angles of ~ 120° (Figure S8A,B).[40,43,50] Finally, the Fourier transform infrared (FTIR) spectrum of $[Fe^{III}(O)Fe^{III}Hpoat]^{2+}$ contained a broad feature at 3224 cm^{-1} that is assigned to a N–H vibration that is in agreement with protonation of one phosphinic amido group (see above, Figure S2B).

Trapping of $[(TMTACN)Fe^{III}–(\mu\text{-}OH)–Fe^{III}poat]^{2+}$.

The isolation of $[Fe^{III}(O)Fe^{III}Hpoat]^{2+}$ was unexpected because the large structural change from $[Fe^{II}(OH)Fe^{III}poat]^{+}$ did not agree with the reversible $Fe^{III}Fe^{III}/Fe^{II}Fe^{III}$ couple found by cyclic voltammetry (Figure 3). Based on the CV, we considered the possibility of whether the initial product of this oxidation was $[(TMTACN)Fe^{III}–(\mu\text{-}OH)–Fe^{III}poat]^{2+}$ ($[Fe^{III}(OH)Fe^{III}poat]^{2+}$) which rearranged during isolation to $[Fe^{III}(O)Fe^{III}Hpoat]^{2+}$.
To evaluate this premise, we attempted to trap $[Fe^{III}(OH)Fe^{III}poat]^{2+}$ by treated $[Fe^{II}(OH)Fe^{III}poat]^{+}$ with $[FeCp_2]OTf$ at −80 °C (Scheme 2), which produced a new species having absorption features at λ_{max} (ε, M^{-1} cm^{-1}) = 330 (8400), 370 (8100), 483 (sh), 513 (1900), 760 nm (300) (Figure S9A,B). Upon warming, these features were replaced by those associated with $[Fe^{III}(O)Fe^{III}Hpoat]^{2+}$ (Figure S9C,D). The Mössbauer spectrum of this new species displayed two doublets from $S = 5/2$ Fe^{III} centers, which were distinct from those of $[Fe^{III}(O)Fe^{III}Hpoat]^{2+}$, with $\delta = 0.34$ mm/s, $|\Delta E_Q| = 0.56$ mm/s and $\delta = 0.44$ mm/s, $|\Delta E_Q| = 0.94$ mm/s (Figure S4D). Furthermore, variable-field and temperature measurements gave $J = 44$ cm^{-1}, which is consistent with the species having an $[Fe^{III}–(\mu\text{-}OH)–Fe^{III}]$ core.[37,38] Taken together, these data indicate that $[Fe^{III}(OH)Fe^{III}poat]^{2+}$ can indeed be trapped at lower temperatures but is unstable at room temperature which leads to the proton transferring to a phosphinic amido group to form $[Fe^{III}(O)Fe^{III}Hpoat]^{2+}$.

Preparation of [(TMTACN)Fe^{III}–(μ-O)–Fe^{III}poat]OTf.

The discovery of [Fe^{III}(O)Fe^{III}Hpoat]$^{2+}$ provided the opportunity to examine whether the phosphinic amide group could be deprotonated to form [(TMTACN)Fe^{III}–(μ-O)–Fe^{III}poat]$^{+}$ ([Fe^{III}(O)Fe^{III}poat]$^{+}$, Scheme 3). We found that treatment of [Fe^{III}(O)Fe^{III}Hpoat]$^{2+}$ with one equivalent of triethylamine caused a change in the absorption spectrum to one with bands at λ_{max} (ε, M^{-1} cm^{-1}) = 349 (9200), 531 (780), and 780 nm (250) (Figure S8C,D). This process is reversible at room temperature: the spectrum associated with [Fe^{III}(O)Fe^{III}Hpoat]$^{2+}$ was regenerated when treated with one equivalent of 2,6-lutidinium triflate (Figure S8E,F). However, features associated with [Fe^{III}(OH)Fe^{III}poat]$^{2+}$ at λ_{max} = 330, 370, 483 (sh), 513, and 760 nm initially appeared when the new species was treated with the same acid at −60 °C (Figure S10A,B); upon warming, the spectrum of [Fe^{III}(O)Fe^{III}Hpoat]$^{2+}$ was obtained (Figure S10C,D). These results are consistent with formation of [Fe^{III}(O)Fe^{III}poat]$^{+}$ in which all the phosphinic amide groups are deprotonated (Scheme 3). Attempts to isolate this new species via this deprotonation route in pure form were unsuccessful because of co-crystallization with the triethylammonium triflate byproduct. We therefore developed an independent synthetic route to this proposed di-Fe species via mixing [Fe^{IV}poat(O)]$^{-}$ with [Fe^{II}(TMTACN)(OTf)$_2$] to produce a pure salt as red crystals (Scheme 4) – the product from the preparation had the identical absorption spectrum as found for the species produced from the deprotonation of [Fe^{III}(O)Fe^{III}Hpoat]$^{2+}$ (Figure S8A,B). The formulation of this species as [Fe^{III}(O)Fe^{III}poat]$^{+}$ was further supported by results obtained by ESI-MS measurements (Figure S7B,C) and FTIR studies that showed a lack of features associated with either an O–H or N–H vibration (Figure S2C). We again used XRD methods to confirm the molecular structure for [Fe^{III}(O)Fe^{III}poat]$^{+}$ (Figure 2C,S5C, Table 1). The structure revealed that the N_4O primary coordination sphere from [poat]$^{3-}$ was restored with all the phosphinic amide arms being deprotonated and their N-atoms coordinated to the Fe^{III} center. This coordination provides a nearly ideal trigonal bipyramidal geometry (τ_5 = 0.950), in contrast to what was observed in [Fe^{III}(O)Fe^{III}Hpoat]$^{2+}$(see above). The Fe^{III} site coordinated to Fe-TMTACN is 6-coordinated with an N_3O_3 primary coordination sphere, consisting of the TMTACN ligand, two O-atoms from the phosphinic amido groups from the [poat]$^{3-}$ ligand, and a bridging oxido ligand. Comparing the structures of [Fe^{III}(O)Fe^{III}Hpoat]$^{2+}$ and [Fe^{III}(O)Fe^{III}poat]$^{+}$ showed that deprotonation had no structural effect on the Fe–(μ-O)–Fe core (Table 1). For instance, the Fe1–O1 and Fe2–O1 bond lengths in the two complexes are statistically equivalent, as are the Fe1…Fe2 separations (3.182(1) and 3.161(1) Å) and Fe1–O1–Fe2 bond angles (124.73(8) and 123.82(10)°). The phosphinic amido group that once participated in forming an intramolecular H-bond (Figure 2A for [Fe^{II}(OH)Fe^{III}poat]$^{+}$) is tilted away from the oxido ligand in [Fe^{III}(O)Fe^{III}poat]$^{+}$ presumably because of electrostatic repulsion (note that the O1···O2 distance is 3.212(3) Å).

The Mössbauer spectrum of [^{57}Fe^{III}(O)^{57}Fe^{III}poat]$^{+}$ contains two distinct doublets with δ = 0.38 mm/s and $|\Delta E_Q|$ = 1.16 mm/s and δ = 0.53 mm/s and $|\Delta E_Q|$ = 1.86 mm/s (Figure S4E). These parameters are consistent with high spin S = 5/2 Fe^{III} centers, and the silent EPR spectrum supports an S = 0 ground state. Variable temperature Mössbauer measurements gave J > 100 cm^{-1}, which is consistent with a Fe–(μ-O)–Fe core.[37,38]

Higher Valent Species: [(TMTACN)Fe^{III}–(μ-O)–Fe^{IV}poat]$^{2+}$.

The isolation of [Fe^{III}(O)Fe^{III}poat]$^{+}$ provided the opportunity to investigate more oxidized di-Fe species. Evidence was provided from cyclic voltammetry studies on [Fe^{III}(O)Fe^{III}poat]$^{+}$ which exhibited a reversible one-electron redox event at +0.55 V, which is assigned to the $Fe^{III}Fe^{IV}/Fe^{III}Fe^{III}$ couple (Figure 4A). The reversibility of the electrochemical event and the relatively moderate potential suggested the one-electron oxidized species can be accessed by a chemical oxidant. Therefore, the treatment of [Fe^{III}(O)Fe^{III}poat]$^{+}$ with one equivalent of [N(*p*-$C_6H_4Br)_3$]PF_6 ($E_{1/2}$ = + 0.70 V vs. [$FeCp_2$]$^{+/0}$ in CH_2Cl_2)[39] at −90°C in CH_2Cl_2 was monitored spectrophotometrically, and produced a new species with absorbance features at λ_{max} = 440 (sh), 515 (sh), 620 (2700), 810 (sh), ~1100 nm (Scheme 5, Figure 4B).

Support for this assignment came from EPR and Mössbauer results. The EPR spectrum of [Fe^{III}(O)Fe^{IV}poat]$^{2+}$ revealed an isotropic S = 1/2 signal centered at g ~ 2.01 that quantified to 92% of the expected concentration (5 mM, Figure 4C). The [Fe^{III}(O)Fe^{IV}poat]$^{2+}$ complex displayed a Mössbauer spectrum of an S = 1/2 antiferromagnetically coupled system (88% yield) containing a high spin Fe^{IV} and Fe^{III} centers, with δ = 0.00 mm/s, ΔE_Q = +0.53 mm/s and δ = 0.46 mm/s, ΔE_Q = −1.11 mm/s, respectively (Figure S4F). The spectrum recorded at high temperature did not collapse to doublets. Thus, these values were determined from simulations of the paramagnetic spectra recorded at multiple magnetic fields; details for these studies will be discussed in a later paper. The value of δ for the Fe^{III} site is close to the values observed for the Fe^{III}(TMTACN) site of the di-Fe^{III} complexes. As a result, we assign the oxidation at the Fe center within [poat]$^{3-}$ to give the formulation of [Fe^{III}(O)Fe^{IV}poat]$^{2+}$. This assignment is consistent with the differences in charge between [poat]$^{3-}$ and TMTACN and our previous discovery that the five-coordinate [Fe^{IV}poat(O)]$^{-}$ complex is high spin.[22,32,51]

Reactivity.

We sought to investigate the reactivity of [Fe^{III}(O)Fe^{IV}poat]$^{2+}$ towards organic substrates that have cleavable X–H bonds (X = N, O, Scheme 6). Initial studies used 1,2-diphenylhydrazine (DPH, $BDFE_{N–H}$(DMSO) = 64.0 kcal mol^{-1})[52] which when allowed to react with [Fe^{III}(O)Fe^{IV}poat]$^{2+}$ at −90°C showed optical changes that are consistent with formation of [Fe^{III}(OH)Fe^{III}poat]$^{2+}$ (λ_{max} = 483, 513, 760 nm, Figure S12A,B). Upon warming, the hydroxido-bridged species further converted to [Fe^{III}(O)Fe^{III}Hpoat]$^{2+}$ with diagonstic features at λ_{max} = 517 and 705 nm (Figure S12C,D). The organic product azobenzene was identified using NMR spectroscopy and gas chromatography-mass spectrometry (GC-MS), and the absence of DPH in both methods supports the full conversion of DPH to azobenzene (Figures S13,14). These findings indicate that DPH undergoes initial proton-coupled electron transfer (PCET) in which proton transfer first occurs at the oxido ligand to form a bridging hydroxido ligand, and electron transfer occurs to reduce the Fe^{IV} center to Fe^{III}. Warming the reaction mixture to room temperature promotes an intramolecular proton transfer from the hydroxido ligand to one of the phosphinic amido groups to form [Hpoat]$^{2-}$ as we have observed previously.

We also explored the reactivity of $[Fe^{III}(O)Fe^{IV}poat]^{2+}$ with phenols to model the mechanistic steps proposed to occur in RNR R2 Class Ia whereby intermediate with an Fe^{IV}-(μ-O)-Fe^{III} core (denoted X) is kinetically competent to cleave the O–H bond of a nearby tyrosine residue.[11,20] Addition of excess 2,6-di-*tert*-butyl-phenol (DTBP, $BDFE_{O-H}(C_6H_6)$ = 77.0 kcal mol^{-1})[52] at −90°C in CH_2Cl_2 caused the features associated with $[Fe^{III}(O)Fe^{IV}poat]^{2+}$ to slowly disappeared at a rate of k_{obs} = 0.0013(2) s^{-1} (Figure S15A,C). Monitoring this process spectrophotometrically produced an absorption spectrum with bands that resembles those of $[Fe^{III}(OH)Fe^{III}poat]^{2+}$ but the spectrum was complicated by additional, unidentified features at λ_{max} = 650 (sh) and >1100 nm. Support for the consumption of $[Fe^{III}(O)Fe^{IV}poat]^{2+}$ during the reaction comes from the disappearance of its characteristic isotropic EPR feature g = 2.01. Moreover, warming the reaction mixture to room temperature produced the diagnostic absorption spectrum of $[Fe^{III}(O)Fe^{III}Hpoat]^{2+}$ (Figure S15B). The organic products, 3,3',5,5'-tetra-*tert*-butyl[1,1'-biphenyl]-4,4'-diol (bisphenol) and 3,3',5,5'-tetra-*tert*-butyldiphenoquinone (diphenoquinone), were detected by GC-MS with a combined conversion of greater than 90 % (Figure S16). These results suggest DTBP undergoes PCET with $[Fe^{III}(O)Fe^{IV}poat]^{2+}$ to initially produce $[Fe^{III}(OH)Fe^{III}poat]^{2+}$ and the corresponding phenoxyl radical. 2,6-*tert*-Butyl-phenoxyl radical is known to react through bimolecular homo-coupling at the para-position to produce bisphenol,[53–55] which further reacts with remaining $[Fe^{III}(O)Fe^{IV}poat]^{2+}$ to produce diphenoquinone (Scheme 6).[56,57]

Discussion

Spanning 4 Oxidation States.

Di-Fe cores within the active sites of metalloproteins are known to access a variety of oxidation levels during turnover that are often accompanied by structural modifications.[18] The active site within RNR R2 is an example and is known to proceed through a series of oxidation steps from an di-Fe^{II} core to one that contains an $Fe^{IV}Fe^{III}$ center (intermediate X).[10–13,20,21] To investigate these types of oxidation steps and their associated structural changes, we developed a series of synthetic di-Fe complexes in which the properties at each oxidation level from di-Fe^{II} to $Fe^{IV}Fe^{III}$ were examined (Scheme 7; Table 2). Their preparation was initiated using an assembly approach that coupled the Fe^{III}–OH complex $[Fe^{III}poat(OH)]^-$ with $[Fe^{II}(TMTACN)(OTf)_2]$ to form the bimetallic complex $[Fe^{II}(OH)Fe^{III}poat]^+$. This mixed valent complex exhibited two reversible redox events (Figure 3) that allow access to both the one-electron reduced and oxidized analogs. The most reduced state, $[Fe^{II}(OH)Fe^{II}poat]$ was accessed by chemical reduction and we were able to trap the oxidized $[Fe^{III}(OH)Fe^{III}poat]^{2+}$ at low temperatures. However, we found that this di-Fe^{III} complex was unstable at room temperature and rearranged to $[Fe^{III}(O)Fe^{III}Hpoat]^{2+}$, which can be treated with external bases to produce $[Fe^{III}(O)Fe^{III}poat]^+$ and then chemically oxidize to $[Fe^{III}(O)Fe^{IV}poat]^{2+}$ at −90°C.

Multi-Functional Properties of $[poat]^{3-}$ and Intramolecular Proton Transfer.

The assembly of the di-Fe complexes involved two of the phosphinic amido groups from $[Fe^{III}poat(OH)]^-$ that coordinate another Fe center through their P=O units. Together with the hydroxido/oxido ligand, triply bridged di-Fe cores are produced. Our electrochemical

studies found that the P=O groups can stabilize Fe^{III} centers at relative low potentials, which could not be achieved with related tripodal ligands such as those with sulfonamido groups. The third phosphinic amido arm is distinct from the other two and served multiple functions. In $[Fe^{II}(OH)Fe^{III}poat]^{+}$ it is an H-bond acceptor to promote the formation of an intramolecular bond with the bridging hydroxido ligand. Room temperature oxidation produced the isolatable $[Fe^{III}(O)Fe^{III}Hpoat]^{2+}$ with the distinct arm now serving as a site of protonated at its N-atom. This intramolecular proton transfer (PT) causes formation of an $Fe^{III}–(\mu\text{-}O)–Fe^{III}$ core and a structural rearrangement with the phosphinic amide coordinating to the Fe center through its P=O unit. The dual binding modes of the phosphinic amido/amide thus provides dynamic primary and secondary coordination spheres around the di-Fe core to store a proton and stabilize di-Fe species at different oxidation levels.

Although $[Fe^{III}(O)Fe^{III}Hpoat]^{2+}$ is the product isolated from the room temperature oxidation, our results suggested that the initial species formed is $[Fe^{III}(OH)Fe^{III}poat]^{2+}$ because of the reversibility of this process in the cyclic voltammogram (Scheme 7). Moreover, when the oxidation was done at −80°C, we detect a species whose properties were consistent with $[Fe^{III}(OH)Fe^{III}poat]^{2+}$. We correlated the absorption spectra and the experimentally determined spin exchange constants (J) from Mössbauer measurements to gauge the protonation state of the O-atom bridge in each complex because most di-Fe complexes with bridging hydroxido ligand have J-values of less than 50 cm^{-1}, whereas the values for oxido bridged species are substantially larger ($J > 60$ cm^{-1}).[38] The most reduced form, $[Fe^{II}(OH)Fe^{II}poat]$, has a $J = 20$ cm^{-1}, which supports the assignment of a bridging hydroxido ligand. For $[Fe^{II}(OH)Fe^{III}poat]^{+}$, the J-value increases to 30 cm^{-1}, and upon further oxidation, a J-value of 44 cm^{-1} was determined for $[Fe^{III}(OH)Fe^{III}poat]^{2+}$. The incremental rise in the J values is consistent with the increased Lewis acidity of the Fe centers and Bronsted acidity of the $Fe–(\mu\text{-}OH)–Fe$ core, which results in strengthened intramolecular H-bonding interactions between the OH and the P=O groups, and increased oxido character in the bridging ligand. The J-value obtained for $[Fe^{III}(OH)Fe^{III}poat]^{2+}$ is also larger than those reported for related complexes with $Fe^{III}–(\mu\text{-}OH)–Fe^{III}$ cores – these examples lack an intramolecular H-bond and J-values of ~34 cm^{-1} were measured.[58,59] Finally, both $[Fe^{III}(O)Fe^{III}Hpoat]^{2+}$ and $[Fe^{III}(O)Fe^{III}poat]^{+}$ had J-values of greater than 100 cm^{-1} that are consistent with oxido-bridged di-Fe cores.[38]

The factors that regulate between oxido and hydroxido bridging ligands within di-Fe species is often difficult to evaluate because $Fe^{III}–(\mu\text{-}OH)–Fe^{III}$ cores are usually not stable enough to observed. For synthetic systems, there are a few examples in which both forms are known, and the magnetic coupling follows the same trend as we observed with our di-Fe^{III} complexes (see above). For metalloproteins, we are not aware of an example in which a di-Fe^{III} core contains a single hydroxido-bridge as is found in $[Fe^{III}(OH)Fe^{III}poat]^{2+}$. With this said, we recognize that our complex is only stable at lower temperature, and at room temperature where most metalloproteins function, it converts to $[Fe^{III}(O)Fe^{III}Hpoat]^{2+}$. However, there is precedent within metalloprotein active sites for coupling PT involving an oxido/hydroxido bridging ligand with electron transfer processes at di-Fe cores. We point to the respiratory protein hemerythrin whereby the resting state $Fe^{II}–(\mu\text{-}OH)–Fe^{II}$ core converts to $Fe^{III}–(\mu\text{-}O)–Fe^{III}(OOH)$, with the proton on the hydroxido bridge being transferred to

the peroxido adduct during oxygenation (Scheme 8A); the proton is transferred back to reform the hydroxido bridge upon deoxygenation.[8,60] This reversibly PT process is mediated by an intramolecular H-bond between the coordinated hydroperoxido ligand and the di-Fe core. In fact, the translocation of protons within active sites are often regulated by H-bonds that involve either ligands within the primary coordination sphere of the Fe centers or amino acid residues within their secondary coordination sphere.[5,6,61] The PT observed in the di-Fe complexes with $[poat]^{3-}$ is reminiscent of these bioprocesses, in which PT was undoubtedly directed to the distinct phosphinic amido through the H-bonding interaction involving the polarized P=O unit. The transfer of the proton to the O-atom, which is involved in H-bonding, would likely occur first and then tautomerization would afford $[Fe^{III}(O)Fe^{III}Hpoat]^{2+}$ (Scheme 8B). We note that similar to what is found in hemerythrin, reversion of the Fe–(μ-OH)–Fe unit can occur via reduction of $[Fe^{III}(O)Fe^{III}Hpoat]^{2+}$ with cobaltocene to reform $[Fe^{II}(OH)Fe^{III}poat]^{2+}$ (Scheme 7, Figure S17).

Comparison of $[Fe^{III}(O)Fe^{IV}poat]^{2+}$ with Related Complexes.

The oxidation of $[Fe^{III}(O)Fe^{III}poat]^{+}$ to $[Fe^{III}(O)Fe^{IV}poat]^{2+}$ was achieved in good yield (> 80 %), allowing us to perform magnetic studies on this high valent species. The spectroscopic data support the assignment of a mixed valent species having an $S = 1/2$ spin ground state with an isotropic g-tensor of $g = 2.01$ (Figure 4C). This result is consistent with Fe^{IV}–(μ–O)–Fe^{III} cores found in biological and other synthetic systems,[20,23,29,30,62] including the intermediate X in RNR R2. The Mössbauer spectra identified two distinct Fe centers with parameters of valence localized $S = 2$ Fe^{IV} and $S = 5/2$ Fe^{III} sites, and are similar to those previously reported in the literature.[20,23,30,62] The trianionic $[poat]^{3-}$ framework that enforces local C_3 symmetry likely stabilizes high-spin Fe^{IV} center within the tripodal site.[32] There have been reports of the detection and/or isolation of Fe^{IV}–(μ–O)–Fe^{III} species in various ligands;[22,23,25,26,29,30,53,54,63] however, $[Fe^{III}(O)Fe^{IV}poat]^{2+}$ is different in that the bimetallic core is housed within a unsymmetric ligand framework, and both Fe centers are high spin, making the complex a suitable synthetic model for high valent non-heme di-Fe active sites in proteins.

Reactivity Comparison with RNR.

We explored the reactivity of $[Fe^{III}(O)Fe^{IV}poat]^{2+}$ towards external substrates to gain insights into the species that are formed after X–H bond cleavage. DPH and DTBP were used as substrates and in both instances the reaction mixtures show optical changes that are consistent with the generation of $[Fe^{III}(OH)Fe^{III}poat]^{2+}$ at −90°C (Figures S12, S15). The results are consistent with a PCET process, whereby the proton is transferred to the bridging oxido ligand, and the electron is transferred to the Fe^{IV} center. Accessibility thus appears not be the dominant factor for the site of initial proton transfer; our structural work clearly indicates that the oxido ligand is less accessible than the P=O group of the distinct phosphinic amido arm (Figure 2D). We have experimentally verified that the oxido is the initial site of protonation by treating $[Fe^{III}(O)Fe^{III}poat]^{+}$ with an acid at low temperature, which generated $[Fe^{III}(OH)Fe^{III}poat]^{2+}$ (Schemes 3 and 7, Figure S10). Upon warming to room temperature, $[Fe^{III}(OH)Fe^{III}poat]^{2+}$ converts to the more thermally stable $[Fe^{III}(O)Fe^{III}Hpoat]^{2+}$. The organic products in both reactions are consistent with the homolytic cleavage of the X–H bonds to initially form radical species that react further

to give more stable products. This type of process may have relevance to the chemistry observed within the R2 subunit of RNR Class Ia.[10–13] The catalytically competent species, intermediate X, also contains Fe^{IV}–(μ–O)–Fe^{III} core and homolytically cleaves the O–H bond in a nearby tyrosine residue to produce a Fe^{III}–(μ–O)–Fe^{III} core with concomitant generation of a tyrosyl radical.[20] While the electron transfer is established, the translocation of the proton is still not fully understood. One suggestion is for the proton from this process is transferred to a terminally coordinated hydroxido ligand to form an aqua ligand.[2,11,21,64] We suggest a modified version of this mechanism in that the initial site of protonation is the oxido bridge to give an Fe^{III}–(μ–OH)–Fe^{III} core (Scheme 9). Similar to what we observed for $[Fe^{III}(OH)Fe^{III}poat]^{2+}$, intramolecular PT then occurs to form the aqua ligand. This additional PT step helps stabilize the product by retaining the more stable Fe–(μ–O)–Fe core and controlling the proton movement to avoid additional unproductive reactions. Within this context, the active site in RNR and the di-Fe complexes of $[poat]^{3-}$ share similar structural aspects including dynamic coordination spheres that allows for the proton rearrangement for enhanced stability.

Conclusions

Our work demonstrates the utility of the phosphinic amido ligand $[poat]^{3-}$ in assembling and stabilizing complexes with di-Fe cores at a variety of different oxidation levels. While $[poat]^{3-}$ typically binds to one Fe centers through the four N donors, we found the protonated $[Hpoat]^{2-}$ can bind in a N_3O coordination mode, where one phosphinic amide arm is protonated at the N-atom but remains bound *via* the polar P=O group. This change in the ligand structure was triggered by the oxidation of the di-Fe core which caused the bridging hydroxido ligand to convert to an oxido ligand through intramolecular proton transfer. We illustrate that this type of structural modulation allows for proton storage proximal to the Fe–(μ-O)–Fe unit to provide the facile coupling of proton and electron transfer processes. While both $[Hpoat]^{2-}$ and $[poat]^{3-}$ can stabilize complexes with Fe^{III}–(μ-O)–Fe^{III} cores at room temperature, only $[Fe^{III}(O)Fe^{III}poat]^{+}$ was able to be further oxidized to an $Fe^{IV}Fe^{III}$ species which we used to probe for reactivity towards substrates containing cleavable X–H bonds. From our studies, we proposed a modified mechanism for the catalytic turnover in the R2 subunit of RNR, in which the oxido bridge first accepts the proton upon homolytic cleavage of the tyrosine O–H bond, before the di-Fe core undergoes an intramolecular proton transfer. These mechanistic insights emphasize the importance to consider both proton and electron movements in reactions observed for biological and synthetic systems.

Supplementary Material

Refer to Web version on PubMed Central for supplementary material.

ACKNOWLEDGMENT

The authors acknowledge the NIH (GM050781 to A.S.B., GM077387 to M.P.H.) for funding and the UCI Department of Chemistry for fellowships to J.L.L. and C.S.

References

(1). Reece SY; Nocera DG Proton-Coupled Electron Transfer in Biology: Results from Synergistic Studies in Natural and Model Systems. Annu. Rev. Biochem. 2009, 78, 673–699. [PubMed: 19344235]

(2). Migliore A; Polizzi NF; Therien MJ; Beratan DN Biochemistry and Theory of Proton-Coupled Electron Transfer. Chem. Rev. 2014, 114, 3381–3465. [PubMed: 24684625]

(3). Gray HB; Winkler JR Hole Hopping through Tyrosine/Tryptophan Chains Protects Proteins from Oxidative Damage. Proc. Natl. Acad. Sci. U. S. A. 2015, 112, 10920–10925. [PubMed: 26195784]

(4). Warren JJ; Mayer JM Moving Protons and Electrons in Biomimetic Systems. Biochemistry 2015, 54, 1863–1878. [PubMed: 25742166]

(5). Shook RL; Borovik AS Role of the Secondary Coordination Sphere in Metal-Mediated Dioxygen Activation. Inorg. Chem. 2010, 49, 3646–3660. [PubMed: 20380466]

(6). Cook SA; Hill EA; Borovik AS Lessons from Nature: A Bio-Inspired Approach to Molecular Design. Biochemistry 2015, 54, 4167–4180. [PubMed: 26079379]

(7). Span EA; Suess DLM; Deller MC; Britt RD; Marletta MA The Role of the Secondary Coordination Sphere in a Fungal Polysaccharide Monooxygenase. ACS Chem. Biol. 2017, 12, 1095–1103. [PubMed: 28257189]

(8). Klotz IM; Kurtz DM Binuclear Oxygen Carriers: Hemerythrin. Acc. Chem. Res. 1984, 17, 16–22.

(9). Tinberg CE; Lippard SJ Dioxygen Activation in Soluble Methane Monooxygenase. Acc. Chem. Res. 2011, 44, 280–288. [PubMed: 21391602]

(10). Nordlund P; Reichard P Ribonucleotide Reductases. Annu. Rev. Biochem. 2006, 75, 681–706. [PubMed: 16756507]

(11). Minnihan EC; Nocera DG; Stubbe J Reversible, Long-Range Radical Transfer in *E. Coli* Class Ia Ribonucleotide Reductase. Acc. Chem. Res. 2013, 46, 2524–2535. [PubMed: 23730940]

(12). Kang G; Taguchi AT; Stubbe J; Drennan CL Structure of a Trapped Radical Transfer Pathway within a Ribonucleotide Reductase Holocomplex. Science, 2020, 368, 424–427. [PubMed: 32217749]

(13). Greene BL; Kang G; Cui C; Bennati M; Nocera DG; Drennan CL; Stubbe J Ribonucleotide Reductases: Structure, Chemistry, and Metabolism Suggest New Therapeutic Targets. Annu. Rev. Biochem. 2020, 89, 45–75. [PubMed: 32569524]

(14). Caranto JD; Weitz A; Giri N; Hendrich MP; Kurtz DM A Diferrous-Dinitrosyl Intermediate in the N_2O-Generating Pathway of a Deflavinated Flavo-Diiron Protein. Biochemistry 2014, 53, 5631–5637. [PubMed: 25144650]

(15). Hayashi T; Caranto JD; Wampler DA; Kurtz DM; Moënne-Loccoz P Insights into the Nitric Oxide Reductase Mechanism of Flavodiiron Proteins from a Flavin-Free Enzyme. Biochemistry 2010, 49, 7040–7049. [PubMed: 20669924]

(16). Fox BG; Shanklintt J; Somervillet C; Münck E Stearoyl-Acyl Carrier Protein Δ^9 Desaturase from *Ricinus Communis* Is a Diiron-Oxo Protein. Proc. Natl. Acad. Sci. U. S. A. 1993, 90, 2486–2490. [PubMed: 8460163]

(17). Yang Y-S; Broadwater JA; Pulver SC; Fox BG; Solomon EI Circular Dichroism and Magnetic Circular Dichroism Studies of the Reduced Binuclear Non-Heme Iron Site of Stearoyl-ACP Δ^9-Desaturase: Substrate Binding and Comparison to Ribonucleotide Reductase. J. Am. Chem. Soc. 1999, 121, 2770–2783.

(18). Jasniewski AJ; Que L Dioxygen Activation by Nonheme Diiron Enzymes: Diverse Dioxygen Adducts, High-Valent Intermediates, and Related Model Complexes. Chem. Rev. 2018, 118, 2554–2592. [PubMed: 29400961]

(19). Kurtz DM Structural Similarity and Functional Diversity in Diiron-Oxo Proteins. J. Biol. Inorg. Chem. 1997, 2, 159–167.

(20). Sturgeon BE; Burdi D; Chen S; Huynh B-H; Edmondson DE; Stubbe J; Hoffman BM Reconsideration of X, the Diiron Intermediate Formed during Cofactor Assembly in *E. Coli* Ribonucleotide Reductase. J. Am. Chem. Soc. 1996, 118, 7551–7557.

(21). Doan PE; Shanmugam M; Stubbe J; Hoffman BM Composition and Structure of the Inorganic Core of Relaxed Intermediate X (Y122F) of Escherichia Coli Ribonucleotide Reductase. J. Am. Chem. Soc. 2015, 137, 15558–15566. [PubMed: 26636616]

(22). Slep LD; Mijovilovich A; Meyer-Klaucke W; Weyhermüller T; Bill E; Bothe E; Neese F; Wieghardt K Mixed-Valent {FeIV(μ-O)(μ-Carboxylato)2FeIII}3+ Core. J. Am. Chem. Soc. 2003, 125, 15554–15570. [PubMed: 14664603]

(23). Lee D; Pierce B; Krebs C; Hendrich MP; Huynh BH; Lippard SJ Functional Mimic of Dioxygen-Activating Centers in Non-Heme Diiron Enzymes: Mechanistic Implications of Paramagnetic Intermediates in the Reactions between Diiron(II) Complexes and Dioxygen. J. Am. Chem. Soc. 2002, 124, 3993–4007. [PubMed: 11942838]

(24). Ghosh A; Tiago de Oliveira F; Yano T; Nishioka T; Beach ES; Kinoshita I; Münck E; Ryabov AD; Horwitz CP; Collins TJ Catalytically Active μ-Oxodiiron(IV) Oxidants from Iron(III) and Dioxygen. J. Am. Chem. Soc. 2005, 127, 2505–2513. [PubMed: 15725005]

(25). Wang D; Farquhar ER; Stubna A; Münck E; Que L A Diiron(IV) Complex That Cleaves Strong C–H and O–H Bonds. Nat. Chem. 2009, 1, 145–150. [PubMed: 19885382]

(26). Hsu H-F; Dong Y; Shu L; Young VG; Que L Crystal Structure of a Synthetic High-Valent Complex with an Fe2(μ-O)2 Diamond Core. Implications for the Core Structures of Methane Monooxygenase Intermediate Q and Ribonucleotide Reductase Intermediate X. J. Am. Chem. Soc. 1999, 121, 5230–5237.

(27). Xue G; Wang D; De Hont R; Fiedler AT; Shan X; Münck E; Que L A Synthetic Precedent for the [FeIV2(μ-O)2] Diamond Core Proposed for Methane Monooxygenase Intermediate Q. Proc. Natl. Acad. Sci. U. S. A. 2007, 104, 20713–20718. [PubMed: 18093922]

(28). Xue G; Fiedler AT; Martinho M; Munck E; Que LJ Insights into the P-to-Q Conversion in the Catalytic Cycle of Methane Monooxygenase from a Synthetic Model System. Proc. Natl. Acad. Sci. U. S. A. 2008, 105, 20615–20620.

(29). Xue G; De Hont R; Münck E; Que L Million-Fold Activation of the [Fe2(μ-O)2] Diamond Core for C-H Bond Cleavage. Nat. Chem. 2010, 2, 400–405. [PubMed: 20414242]

(30). De Hont RF; Xue G; Hendrich MP; Que L; Bominaar EL; Münck E Mössbauer, Electron Paramagnetic Resonance, and Density Functional Theory Studies of Synthetic $S = 1/2$ Fe^{III}-O-Fe^{IV}=O Complexes. Superexchange-Mediated Spin Transition at the Fe^{IV}=O Site. Inorg. Chem. 2010, 49, 8310–8322. [PubMed: 20795646]

(31). Stoian SA; Xue G; Bominaar EL; Que L; Münck E Spectroscopic and Theoretical Investigation of a Complex with an [O═Fe^{IV}-O-Fe^{IV}═O] Core Related to Methane Monooxygenase Intermediate Q. J. Am. Chem. Soc. 2014, 136, 1545–1558. [PubMed: 24380398]

(32). Oswald VF; Lee JL; Biswas S; Weitz AC; Mittra K; Fan R; Li J; Zhao J; Hu MY; Alp EE; Bominaar EL; Guo Y; Green MT; Hendrich MP; Borovik AS Effects of Noncovalent Interactions on High-Spin Fe(IV)–Oxido Complexes. J. Am. Chem. Soc. 2020, 142, 11804–11817. [PubMed: 32489096]

(33). Sano Y; Weitz AC; Ziller JW; Hendrich MP; Borovik AS Unsymmetrical Bimetallic Complexes with MII–(μ-OH)–MIII Cores (MIIMIII = FeIIFeIII, MnIIFeIII, MnIIMnIII): Structural, Magnetic, and Redox. Inorg. Chem. 2013, 52, 10229–10231. [PubMed: 23992041]

(34). Sano Y; Lau N; Weitz AC; Ziller JW; Hendrich MP; Borovik AS Models for Unsymmetrical Active Sites in Metalloproteins: Structural, Redox, and Magnetic Properties of Bimetallic Complexes with MII-(μ-OH)-FeIII Cores. Inorg. Chem. 2017, 56, 14118–14128. [PubMed: 29112385]

(35). Lee JL; Oswald VF; Biswas S; Hill EA; Ziller JW; Hendrich MP; Borovik AS Stepwise Assembly of Heterobimetallic Complexes: Synthesis, Structure, and Physical Properties. Dalt. Trans. 2021, 50, 8111–8119.

(36). Lee JL; Ross DL; Barman SK; Ziller JW; Borovik AS C-H Bond Cleavage by Bioinspired Nonheme Metal Complexes. Inorg. Chem. 2021, 60, 13759–13783. [PubMed: 34491738]

(37). Tshuva EY; Lippard SJ Synthetic Models for Non-Heme Carboxylate-Bridged Diiron Metalloproteins: Strategies and Tactics. Chem. Rev. 2004, 104, 987–1012. [PubMed: 14871147]

(38). Kurtz DM Oxo- and Hydroxo-Bridged Diiron Complexes: A Chemical Perspective on a Biological Unit. Chem. Rev. 1990, 90, 585–606.

(39). Connelly NG; Geiger WE Chemical Redox Agents for Organometallic Chemistry. Chem. Rev. 1996, 96, 877–910. [PubMed: 11848774]

(40). Wieghardt K; Pohl K; Gebert W [{(C6H15N3)Fe}2(μ-O)(μ-CH3CO2)2]2+, a Dinuclear Iron(III) Complex with a Metazidohemerythrin-Type Structure. Angew. Chemie Int. Ed. 1983, 22, 727.

(41). Hotzelmann R; Wieghardt K; Flörke U; Haupt H-J; Weatherburn DC; Bonvoisin J; Blondin G; Girerd J-J Spin Exchange Coupling in Asymmetric Heterodinuclear Complexes Containing the μ-Oxo-Bis(μ-Acetato)Dimetal Core. J. Am. Chem. Soc. 1992, 114, 1681–1696.

(42). Armstrong WH; Lippard SJ (μ-Oxo)Bis(μ-Acetato)Bis(Tri-1-Pyrazolylborato)Diiron(III), [(HBpz3)FeO(CH3CO2)2Fe(HBpz3)]: Model for the Binuclear Iron Center of Hemerythrin. J. Am. Chem. Soc. 1983, 105, 4837–4838.

(43). Armstrong WH; Spool A; Papaefthymiou GC; Frankel RB; Lippard SJ Assembly and Characterization of an Accurate Model for the Diiron Center in Hemerythrin. J. Am. Chem. Soc. 1984, 106, 3653–3667.

(44). Stubna A; Jo D; Costas M; Brenessel WW; Andres H; Bominaar EL; Münck E; Que L A Structural and Mössbauer Study of Complexes with Fe2(μ-O(H))2 Cores: Stepwise Oxidation from FeII(μ-OH)2FeII through FeII(μ-OH)2FeIII to FeIII(μ-O)(μ-OH)FeIII. Inorg. Chem. 2004, 43, 3067–3079. [PubMed: 15132612]

(45). Kryatov SV; Taktak S; Korendovych IV; Rybak-Akimova EV; Kaizer J; Torelli S; Shan X; Mandal S; MacMurdo VL; Mairata i Payeras A; Que L Dioxygen Binding to Complexes with FeII2(μ-OH)2 Cores: Steric Control of Activation Barriers and O2-Adduct Formation. Inorg. Chem. 2005, 44, 85–99. [PubMed: 15627364]

(46). Chaudhuri P; Wieghardt K; Nuber B; Weiss J [L2Fe2II(μ-OH)(μ-CH3CO2)2](ClO4)·H2O, a Model Compound for the Diiron Centers in Deoxyhemerythrin. Angew. Chem., Int. Ed. Engl. 1985, 24, 778–779.

(47). Bossek U; Hummel H; Weyhermüller T; Bill E; Wieghardt K The First μ(OH)-Bridged Model Complex for the Mixed-Valent $Fe^{II}Fe^{III}$ Form of Hemerythrin. Angew. Chem., Int. Ed. Engl. 1996, 34, 2642–2645.

(48). Bradić Z; Harrington PC; Wilkins RG; Yoneda G Role of Mixed Oxidation States in the Oxidation of Hemerythrin Species by Ferricyanide Ion. Biochemistry 1980, 19, 4149–4155. [PubMed: 7417400]

(49). Johnson EJ; Kleinlein C; Musgrave RA; Betley TA Diiron Oxo Reactivity in a Weak-Field Environment. Chem. Sci. 2019, 10, 6304–6310. [PubMed: 31341583]

(50). Sanders-Loehr J; Wheeler WD; Shiemke AK; Averill BA; Loehr TM Electronic and Raman Spectroscopic Properties of Oxo-Bridged Dinuclear Iron Centers in Proteins and Model Compounds. J. Am. Chem. Soc. 1989, 111, 8084–8093.

(51). Note that Wieghardt has been shown that the six-coordinate [FeIVTMTACN(O)]2+ fragment of [(TMTACN)FeIV(μ-O)(μ-OAc)2FeIII(TMTACN)]3+ has an S = 1 spin ground state. See ref 22.

(52). Agarwal RG; Coste SC; Groff BD; Heuer AM; Noh H; Parada GA; Wise CF; Nichols EM; Warren JJ; Mayer JM Free Energies of Proton-Coupled Electron Transfer Reagents and Their Applications. Chem. Rev. 2021, 122, 1–49. [PubMed: 34928136]

(53). Lee D; Du Bois J; Petasis D; Hendrich MP; Krebs C; Huynh BH; Lippard SJ Formation of Fe(III)Fe(IV) Species from the Reaction between a Diiron(II) Complex and Dioxygen: Relevance to Ribonucleotide Reductase Intermediate X. J. Am. Chem. Soc. 1999, 121, 9893–9894.

(54). Kim C; Dong Y; Que L Modeling Nonheme Diiron Enzymes: Hydrocarbon Hydroxylation and Desaturation by a High-Valent Fe_2O_2 Diamond Core. J. Am. Chem. Soc. 1997, 119, 3635–3636.

(55). Mondal P; Pirovano P; Das A; Farquhar ER; McDonald AR Hydrogen Atom Transfer by a High-Valent Nickel-Chloride Complex. J. Am. Chem. Soc. 2018, 140, 1834–1841. [PubMed: 29293330]

(56). Wu T; Macmillan SN; Rajabimoghadam K; Siegler MA; Lancaster KM; Garcia-Bosch I Structure, Spectroscopy, and Reactivity of a Mononuclear Copper Hydroxide Complex in Three Molecular Oxidation States. J. Am. Chem. Soc. 2020, 142, 12265–12276. [PubMed: 32531159]

(57). Türk H; Çimen Y Oxidation of 2,6-Di-Tert-Butylphenol with Tert-Butylhydroperoxide Catalyzed by Cobalt(II) Phthalocyanine Tetrasulfonate in a Methanol-Water Mixture and Formation of an

Unusual Product 4,4′-Dihydroxy-3,3′,5,5′- Tetra-*Tert*-Butylbiphenyl. J. Mol. Catal. A Chem. 2005, 234, 19–24.

(58). Armstrong WH; Lippard SJ Reversible Protonation of the Oxo Bridge in a Hemerythrin Model Compound. Synthesis, Structure, and Properties of (μ-Hydroxo)Bis(μ-Acetato)-Bis[Hydrotris(1-Pyrazolyl)Borato]Diiron(III), [(HB(Pz)3)Fe(OH)(O2CCH3)2Fe(HB(Pz)3)]+. J. Am. Chem. Soc. 1984, 106, 4632–4633.

(59). Wu F-J; Kurtz DM; Hagen KS; Nyman PD; Debrunner PG; Vankai VA (μ-Oxo/Hydroxo)Bis(μ-Carboxylato)Diiron(III) and -Dimanganese(III) Complexes with Capping Tris(Imidazol-2-Yl)Phosphine Ligands. Inorg. Chem. 1990, 29, 5174–5183.

(60). Holmes MA; Le Trong I; Turley S; Sieker LC; Stenkamp RE Structures of Deoxy and Oxy Hemerythrin at 2.0 Å Resolution. J. Mol. Biol. 1991, 218, 583–593. [PubMed: 2016748]

(61). Shiemke AK; Loehr TM; Sanders-Loehr J Resonance Raman Study of Oxyhemerythrin and Hydroxomethemerythrin. Evidence for Hydrogen Bonding of Ligands to the Fe-O-Fe Center. J. Am. Chem. Soc. 1986, 108, 2437–2443. [PubMed: 22175597]

(62). Zheng H; Yoo SJ; Münck E; Que L The Flexible Fe2(μ-O)2 Diamond Core : A Terminal Iron(IV)-Oxo Species Generated from the Oxidation of a Bis(μ-Oxo)Diiron(III) Complex. J. Am. Chem. Soc. 2000, 122, 3789–3790.

(63). Dong Y; Fujii H; Hendrich MP; Leising RA; Pan G; Randall CR; Wilkinson EC; Zang Y; Que L; Fox BG; Kauffmann K; Münck E A High-Valent Nonheme Iron Intermediate. Structure and Properties of [Fe2(μ-O)2(5-Me-TPA)2](ClO4)3. J. Am. Chem. Soc. 1995, 117, 2778–2792.

(64). Shanmugam M; Doan PE; Lees NS; Stubbe J; Hoffman BM Identification of Protonated Oxygenic Ligands of Ribonucleotide Reductase Intermediate X. J. Am. Chem. Soc. 2009, 131, 3370–3376. [PubMed: 19220056]

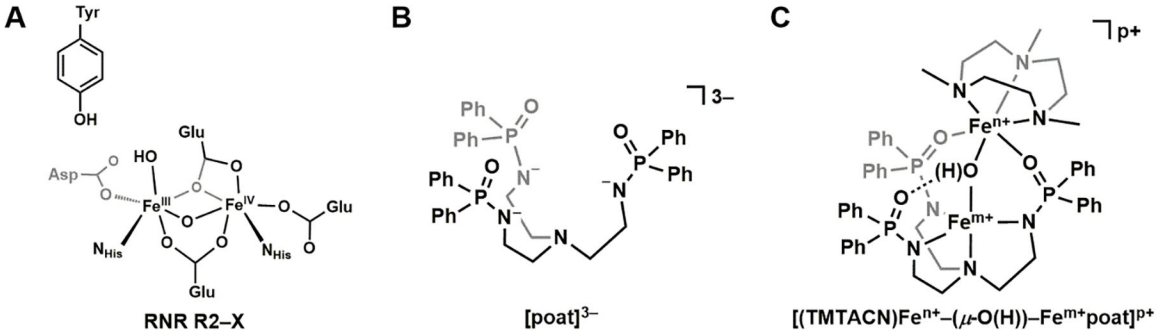

Figure 1.

(A) The proposed chemical structure of Intermediate X in RNR R2. (B) Structure of $[poat]^{3-}$. (C) Structure of a generic $[(TMTACN)Fe^{n+}–(\mu\text{-}O)–Fe^{m+}poat]^{p+}$ complex.

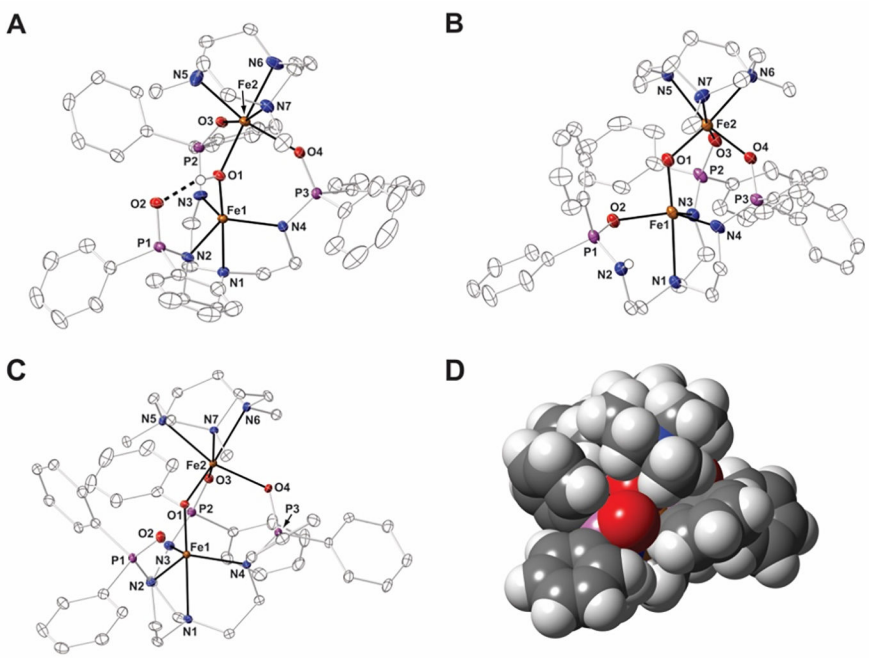

Figure 2.

Thermal ellipsoid diagrams depicting the molecular structures of $[Fe^{II}(OH)Fe^{III}poat]^{+}$ (A), $[Fe^{III}(O)Fe^{III}Hpoat]^{2+}$ (B), $[Fe^{III}(O)Fe^{III}poat]^{+}$ (C), and space-filling model of $[Fe^{III}(O)Fe^{III}poat]^{+}$ (D). Ellipsoids are drawn at the 50 % probability level, and only the hydroxido and phosphinic amide H atoms are shown for clarity. The triflate counter anions are outer-sphere and are not interacting with the cation. The image in (D) illustrates that the P=O group is more accessible than the bridging oxido ligand with the closest red sphere being O2 and the farthest being O1.

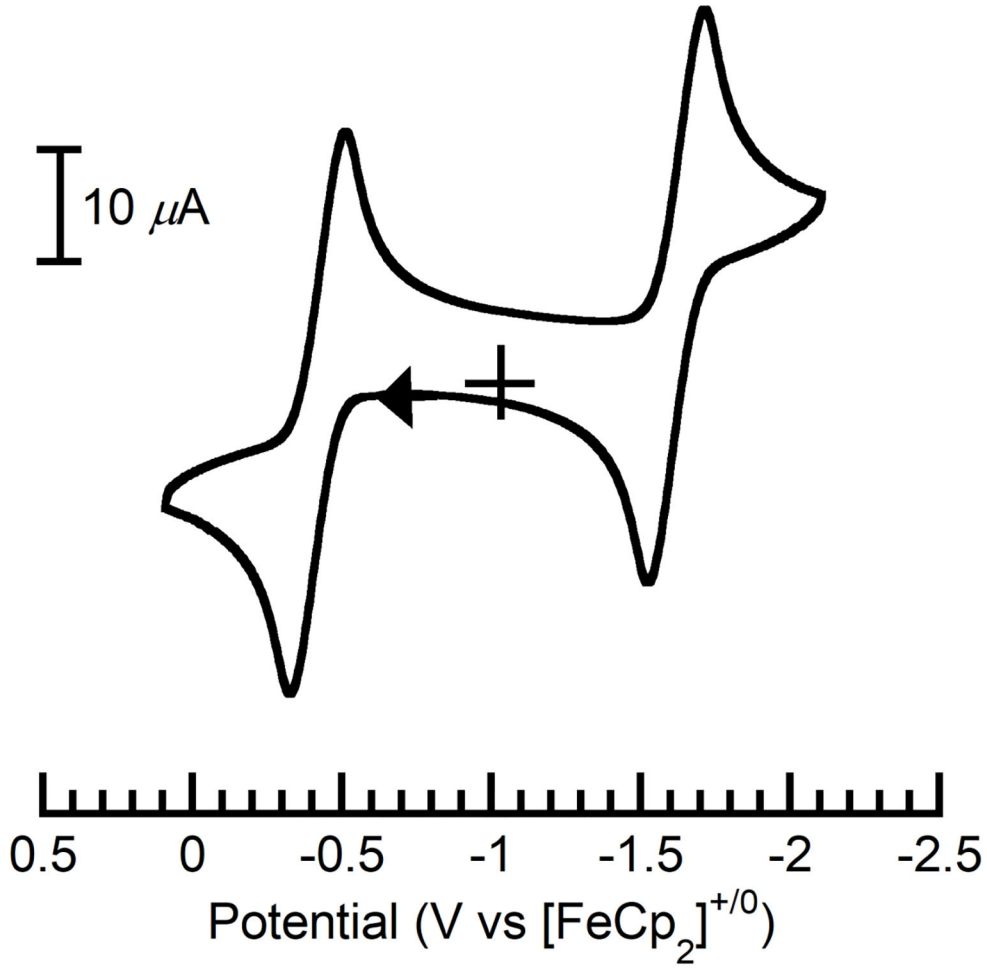

Figure 3.
Cyclic voltammogram of $[Fe^{II}(OH)Fe^{III}poat]^{+}$ collected at scan rate of 100 mV s^{-1} in in CH_2Cl_2.

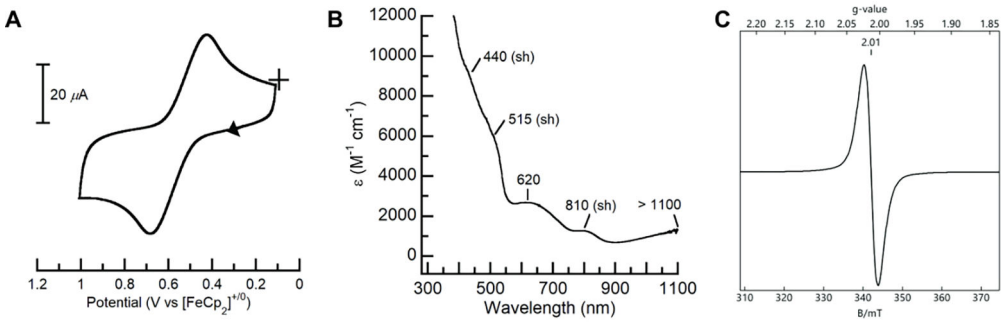

Figure 4.

(A) Cyclic voltammogram of $[Fe^{III}(O)Fe^{III}poat]^{+}$ collected at scan rate of 1 V s^{-1} in in CH2Cl2. (B) Electronic spectrum of $[Fe^{III}(O)Fe^{IV}poat]^{2+}$ at −90 °C. Spectrum collected at 0.20 mM in CH_2Cl_2. (C) EPR spectrum of $[Fe^{III}(O)Fe^{IV}poat]^{2+}$ recorded at 17 K with microwaves of 20 μW at 9.636 GHz.

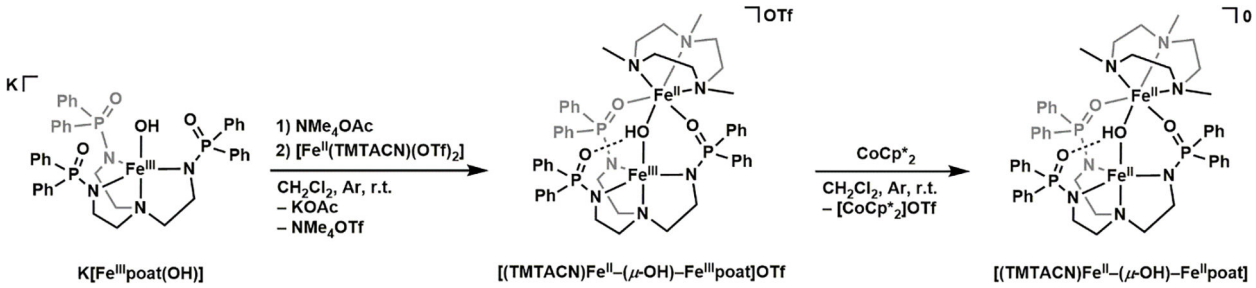

Scheme 1.

Preparative routes for $[Fe^{II}(OH)Fe^{III}poat]^{+}$ and $[Fe^{II}(OH)Fe^{II}poat]$.

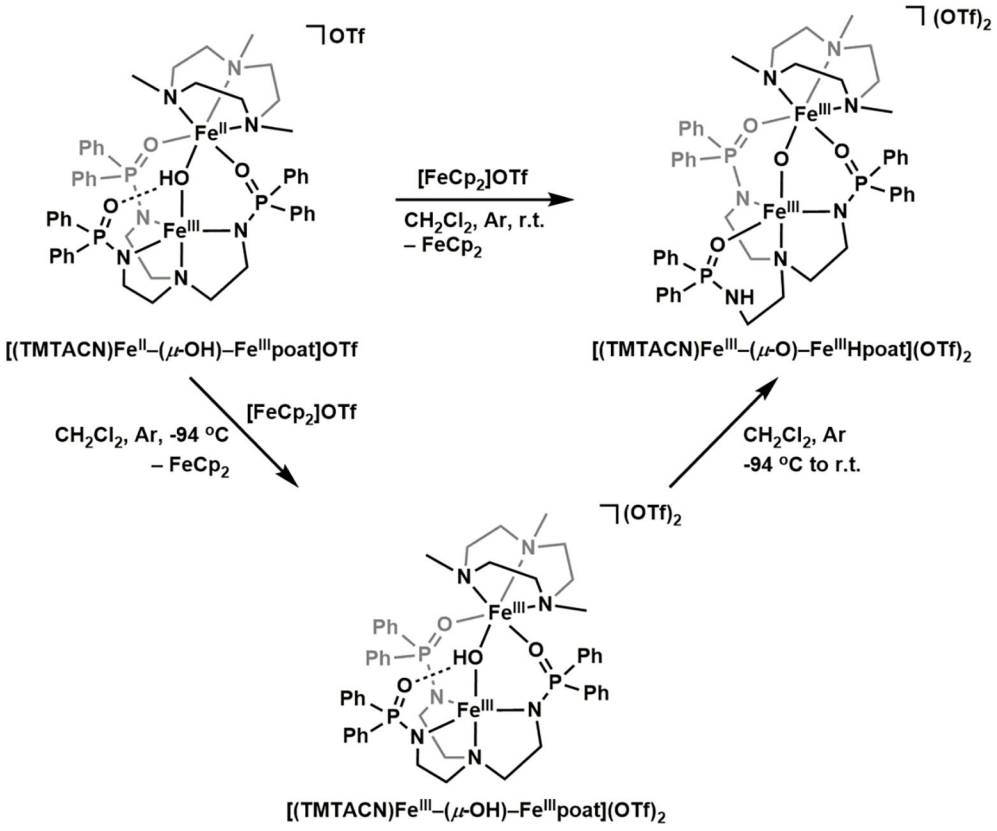

Scheme 2.

Oxidation of $[Fe^{II}(OH)Fe^{III}poat]^{+}$ yields $[Fe^{III}(OH)Fe^{III}poat]^{2+}$, which further converts to $[Fe^{III}(O)Fe^{III}Hpoat]^{2+}$.

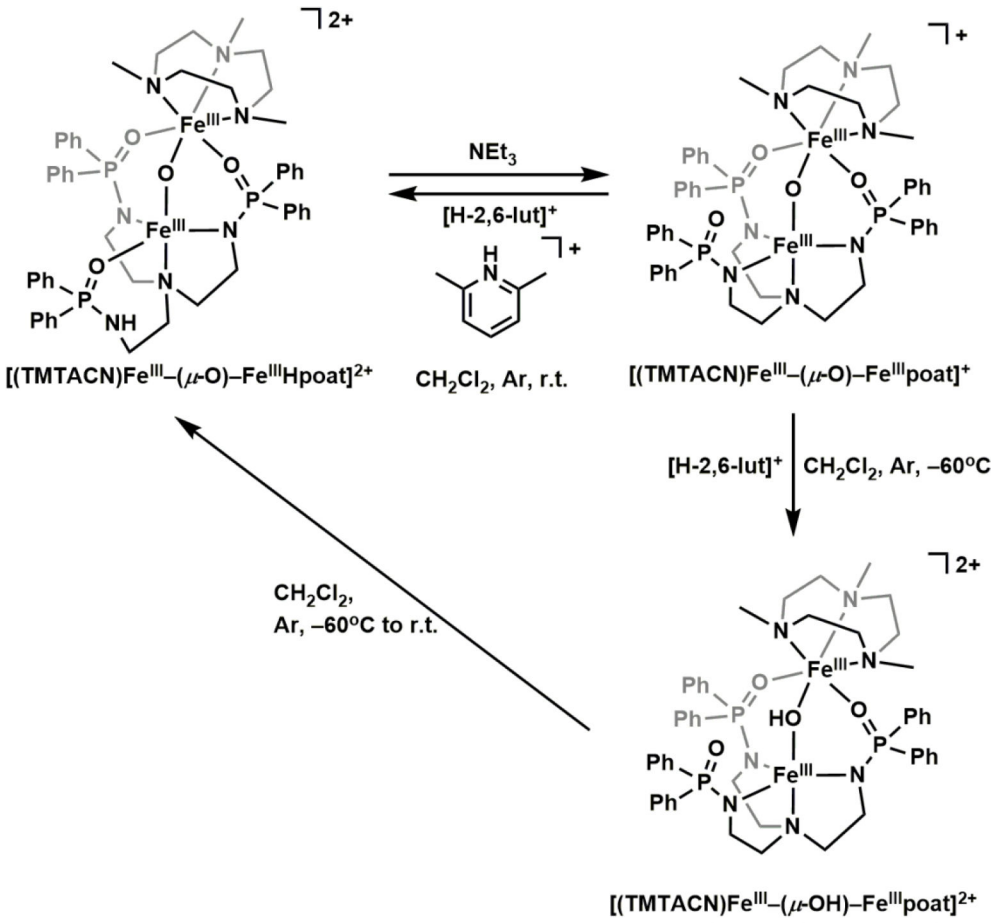

Scheme 3.

Reversible deprotonation and protonation between di-Fe(III) complexes at room and low temperatures.

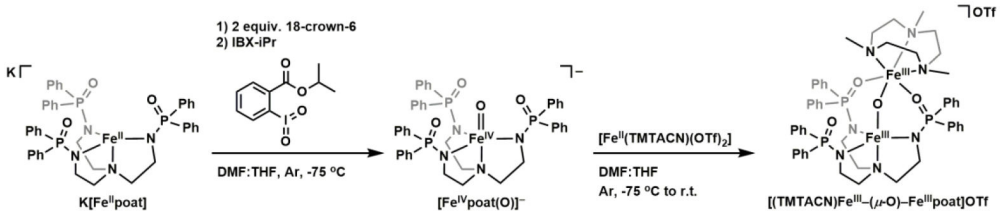

Scheme 4.
Preparative route for $[Fe^{III}(O)Fe^{III}poat]^{+}$.

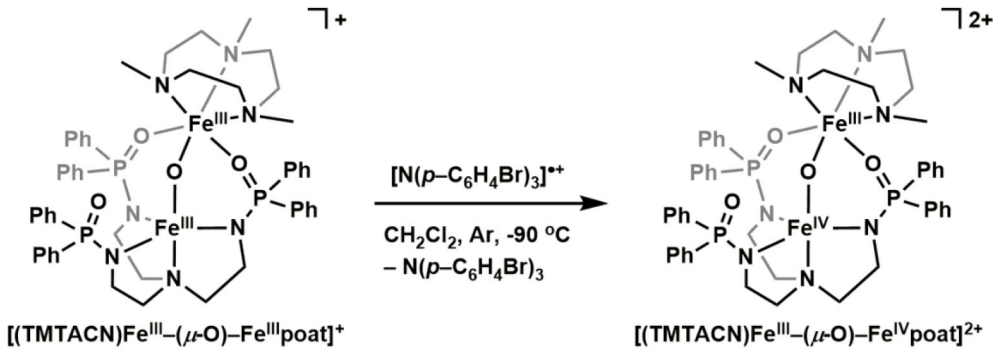

Scheme 5.
Oxidation to $[Fe^{III}(O)Fe^{IV}poat]^{2+}$.

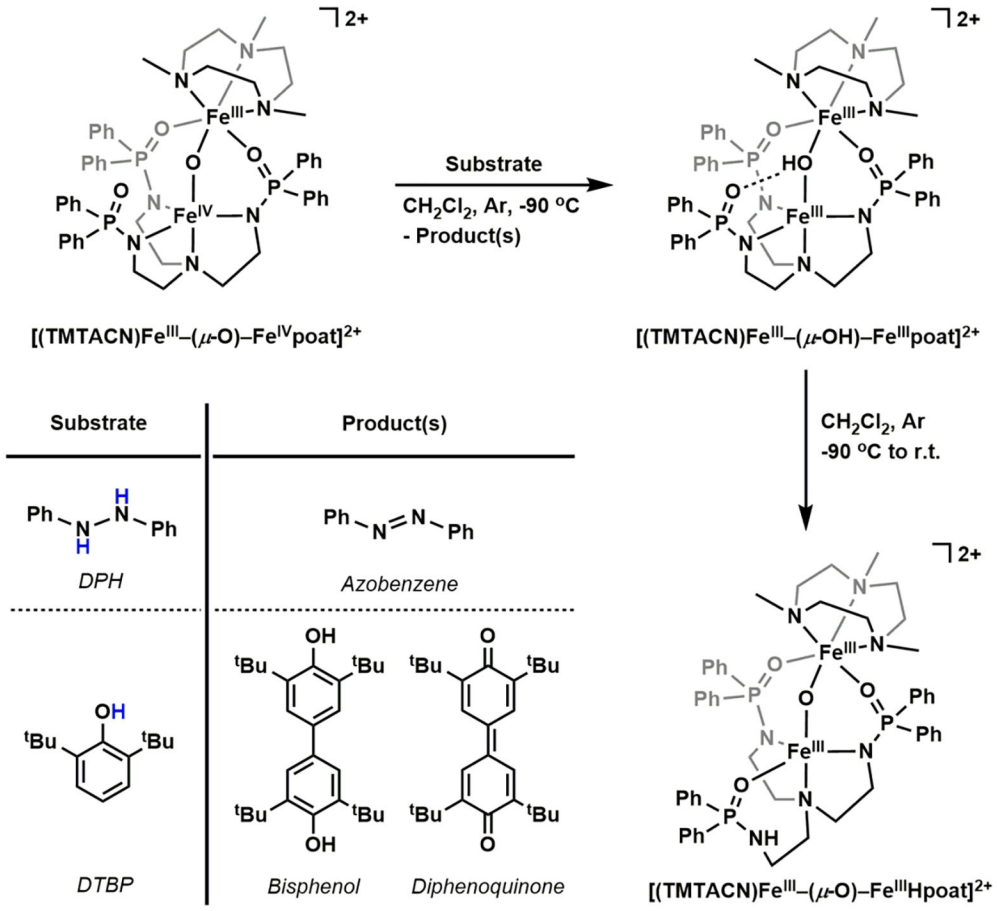

Scheme 6.
Substrate reactivity of $[Fe^{III}(O)Fe^{IV}poat]^{2+}$.

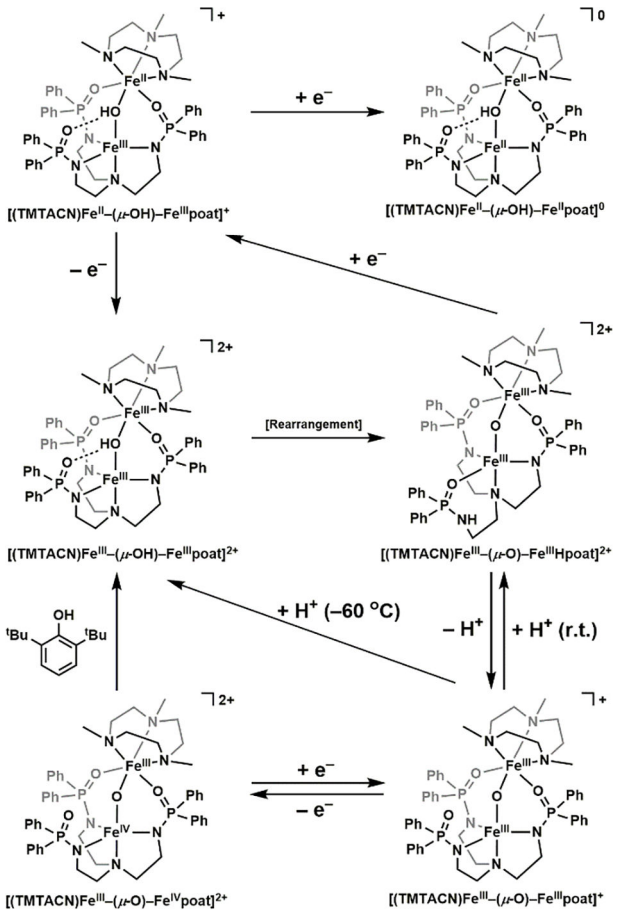

Scheme 7.

Six diiron complexes spanning four oxidation levels and various protonation states.

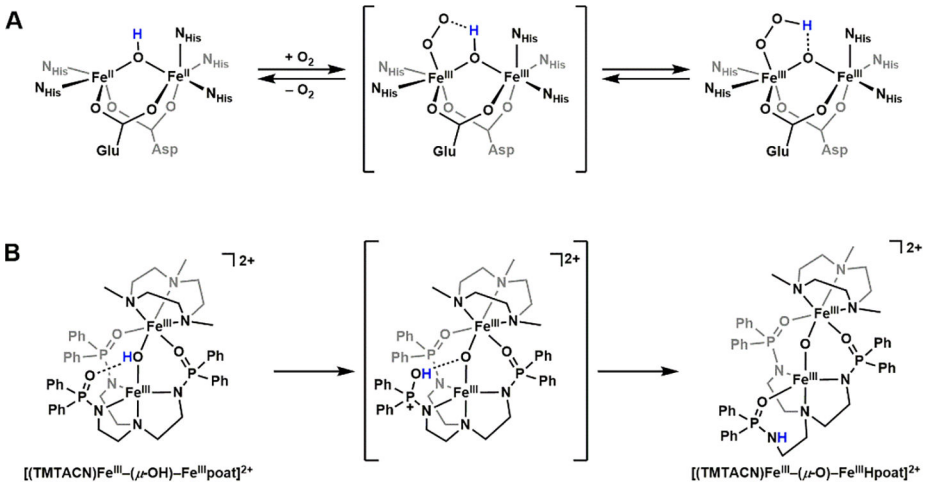

Scheme 8.

(A) Oxygenation of the di-Fe active site in hemerythrin results in the proton transfer from the hydroxido bridge to the peroxido ligand. (B) The thermal unstable $[Fe^{III}(OH)Fe^{III}poat]^{2+}$ converts to $[Fe^{III}(O)Fe^{III}Hpoat]^{2+}$, where the proton likely first transfers to the phosphinic amido O-atom, before residing on the N-atom and the phosphinic amide binds to the Fe center at the O-atom.

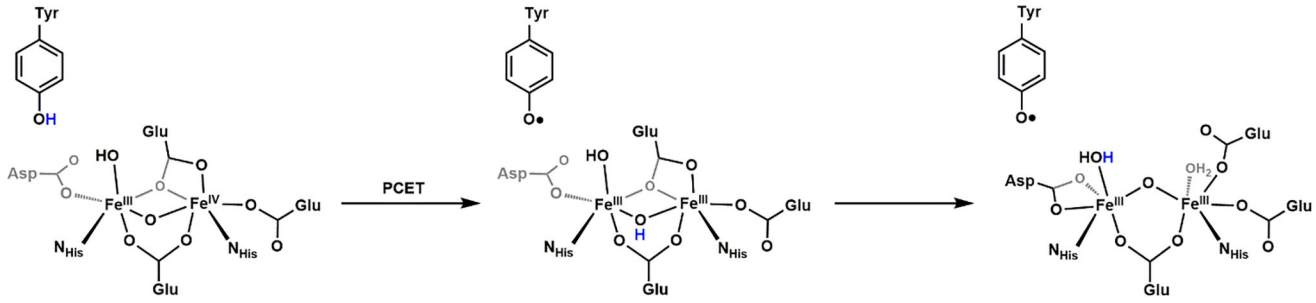

Scheme 9.

Proposed modification to the mechanism in RNR R2 Ia: upon homolytic cleavage of the tyrosine O–H bond, the electron goes to the Fe^{IV} center, and the oxido bridge is first protonated, before the proton transfers to the terminal hydroxido ligand.

Table 1.

Selected bond lengths/distances (Å) and angles (°) for $[Fe^{II}(OH)Fe^{III}poat]^{+}$,[a] $[Fe^{III}(O)Fe^{III}Hpoat]^{2+}$, and $[Fe^{III}(O)Fe^{III}poat]^{+}$

	$[Fe^{II}(OH)Fe^{III}poat]^{+}$	$[Fe^{III}(O)Fe^{III}Hpoat]^{2+}$	$[Fe^{III}(O)Fe^{III}poat]^{+}$
		Bond Distances (Å)	
Fe1–N1	2.210(2)	2.367(2)	2.292(2)
Fe1–N2	2.023(2)	–	2.008(2)
Fe1–O2	–	2.016(1)	–
Fe1–N3	2.011(2)	1.984(2)	2.024(2)
Fe1–N4	2.009(2)	1.999(2)	2.029(2)
Fe1–O1	1.894(l)	1.800(1)	1.799(2)
O1···O2	2.649(2)	–	3.212(3)
Fe2–O1	2.015(2)	1.792(1)	1.784(2)
Fe2–O3	2.094(1)	2.047(1)	2.018(2)
Fe2–O4	2.124(1)	2.002(1)	2.035(2)
Fe2–N5	2.275(2)	2.216(2)	2.231(2)
Fe2–N6	2.213(2)	2.245(2)	2.272(2)
Fe2–N7	2.252(2)	2.223(2)	2.219(2)
Fe1···Fe2	3.436(1)	3.182(1)	3.161(1)
av Fe1–N/O_{eq}	2.014(2)	2.000(2)	2.020(2)
av Fe2–N_{TMTACN}	2.247(2)	2.228(2)	2.241(2)
d[Fe1–N/O_{eq}]	0.363	0.295	0.367
d[Fe2–N_{TMTACN}]	1.522	1.512	1.525
		Bond Angles (deg)	
O1–Fe1–N1	174.52(6)	176.63(6)	179.22(8)
N2–Fe1–N3	119.21(7)	–	122.24(9)
O2–Fe1–N3	–	114.24(6)	–
N3–Fe1–N4	109.71(7)	106.48(7)	107.09(9)
N2–Fe1–N4	121.50(7)	–	120.87(9)
O2–Fe1–N4	–	132.60(6)	–
Fe1–O1–Fe2	123.06(8)	124.73(8)	123.82(10)
O3–Fe2–O4	98.31(5)	98.33(6)	95.72(8)
N5–Fe2–N6	79.50(8)	78.66(6)	77.88(8)
N5–Fe2–N7	78.27(7)	78.90(6)	79.45(8)
N6–Fe2–N7	79.54(6)	79.35(7)	78.94(8)
		Calculated Values	
τ_5 [b]	0.884	0.734	0.950

[a] Bond lengths, distances, and angles are reported as an average.

[b] Trigonality structural parameter, $\tau_5 = (\beta - a)/60°$. β is the largest bond angle observed, and a is the second largest bond angle observed.

Table 2.

Summary of the Spectroscopic Features for the di-Fe Complexes.

Complex	Optical features[a]	S	Fe_{TMTACN}	Fe_{poat}	J[c]
			S ($\delta/\Delta E_Q$)[b]	S ($\delta/\Delta E_Q$)[b]	
$[Fe^{II}(OH)Fe^{III}poat]^+$	315 (sh), 372 (6400), 460 (sh), 520 (sh)	1/2	2 (1.20/−2.84)	5/2 (0.34/−0.72)	30
$[Fe^{II}(OH)Fe^{II}poat]$	350 (sh)	0	2 (1.22/2.37)	2 (1.03/3.38)	20
$[Fe^{III}(O)Fe^{III}Hpoat]^{2+}$	380 (7000), 517 (970), 705 (130)	0	5/2 (0.49/1.83)	5/2 (0.44/1.26)	> 100
$[Fe^{III}(OH)Fe^{III}poat]^{2+}$	330 (8400), 370 (8100), 483 (sh), 513 (1900), 760 (300)	0	5/2 (0.44/0.94)	5/2 (0.34/0.56)	44
$[Fe^{III}(O)Fe^{III}poat]^+$	349 (9200), 531 (780), 780 (250)	0	5/2 (0.53/1.86)	5/2 (0.38/1.16)	> 100
$[Fe^{III}(O)Fe^{IV}poat]^{2+}$	440 (sh), 515 (sh), 620 (2700), 810 (sh), ~ 1100	1/2	5/2 (0.46/−1.11)	2 (0.00/+0.53)	-
$[Fe^{II}poat(OH)]^{2-}$	-	2	-	1.05/3.13	-
$[Fe^{III}poat\ (OH)]^-$[d]	370 (3800)	5/2	-	0.32/0.92	-

[a] λ_{max}, nm (ε, $M^{-1}\ cm^{-1}$).

[b] mm/s.

[c] cm^{-1} ($H = JS_1.S_2$); obtained by Mössbauer.

[d] ref 35